Journal of
Composites Science

MDPI

Article

Microwave Synthesis of Luminescent Recycled Glass Containing Dy_2O_3 and Sm_2O_3

Achanai Buasri, Apichaya Boonpanya, Arraya Yangderm, Thanaporn Kensopha and Vorrada Loryuenyong *

Department of Materials Science and Engineering, Faculty of Engineering and Industrial Technology, Silpakorn University, Nakhon Pathom 73000, Thailand; achanai130@gmail.com (A.B.); boonpanya.150@gmail.com (A.B.); yangdermja@gmail.com (A.Y.); kenso2905@gmail.com (T.K.)
* Correspondence: vorrada@gmail.com; Tel.: +66-034241708

Abstract: This research studied the recycling of borosilicate glass wastes from damaged laboratory glassware. The luminescent glasses were prepared by doping glass waste powder with rare earth ions, namely, dysprosium ions (Dy^{3+}) and samarium ions (Sm^{3+}), as well as co-doping with Dy^{3+} and Sm^{3+} at a concentration of 2% by weight. The sintering process was conducted in a microwave oven for a duration of 15 min. The photoluminescence spectra of the doped glasses were obtained under excitation at 401 nm and 388 nm. The results showed that the emission characteristics depended on the doping concentrations of Dy^{3+} and Sm^{3+} and the excitation wavelengths. Upon excitation at 401 nm, the co-doped glasses exhibited the maximum emission peak of Sm^{3+} at 601 nm (yellowish and orange region in the CIE chromaticity diagram) due to the energy transition from $^4G_{5/2}$ to $^6H_{7/2}$. When excited at 388 nm, however, the emission spectra of the co-doped glasses were similar to the characteristic emission peaks of Dy^{3+} (white region in the CIE chromaticity diagram), but the peak position exhibits a red shift. This could be attributed to an increase in the amount of non-bridging oxygens (NBOs) by co-doping.

Keywords: microwave; dysprosium; samarium; fluorescent glasses; photoluminescence; waste conversion; process innovation

Academic Editor: Heitor Luiz Ornaghi Júnior

Received: 28 December 2024
Revised: 19 January 2025
Accepted: 28 January 2025
Published: 1 February 2025

Citation: Buasri, A.; Boonpanya, A.; Yangderm, A.; Kensopha, T.; Loryuenyong, V. Microwave Synthesis of Luminescent Recycled Glass Containing Dy_2O_3 and Sm_2O_3. *J. Compos. Sci.* **2025**, *9*, 64. https://doi.org/10.3390/jcs9020064

1. Introduction

For thousands of years, glass has been the most widely used packaging material. It is generally non-porous and typically inert with respect to its contents. Moreover, glass is transparent, heat-resistant, and fully recyclable. Waste glass is typically recycled by categorizing it according to its intended purpose. However, the majority of recycled waste glass has mostly been used for the production of bottles and building materials [1]. Although the melting of new glass from recycled materials requires significantly less energy than that of glass from raw materials, additional energy is still required for the recycling processes, which include sorting, cleaning, crushing/grinding, and remelting. It is, therefore, essential to continuously develop technologies to utilize waste glass. For example, it can be employed as a partial or complete replacement for certain materials such as luminescent materials [1–3], aggregates in concrete [4], bricks [5,6], and composite materials [7].

Color tunability of luminescent materials is very desirable in the illumination and display industry. For instance, white light emission may be produced from a combination of three color-emission centers or a combination of blue LEDs and yellow phosphors [8,9]. Previous research has demonstrated the effectiveness of co-doping with a variety of rare earth ions to achieve specific emission characteristics in luminescent materials. Dy^{3+}

typically exhibits two distinct emission peaks: a blue peak at around 480 nm attributed to the $^4F_{9/2} \rightarrow {}^6H_{15/2}$ transition, and a yellow peak at approximately 580 nm corresponding to the $^4F_{9/2} \rightarrow {}^6H_{13/2}$ transition. Sm^{3+}, on the other hand, exhibits an emission peak at approximately 600 nm due to the $^4G_{5/2} \rightarrow {}^6H_{7/2}$ transition. The concentration ratios of Dy^{3+} to Sm^{3+} can be adjusted to produce various emission colors, including the potential for white light emissions [10–12].

W. Yan et al. examined the synthesis and luminescent properties of $NaSrPO_4$ phosphors co-doped with Dy^{3+} and Sm^{3+} ions, which exhibited warm-white luminescence [11]. Upon excitation with UV light at 348 nm, the co-doped phosphors emitted white light, resulting from the combination of two primary emission peaks: one at 484 nm (blue) and another at around 575 nm (orange). The warm-white luminescence was attributed to energy transfer between Dy^{3+} and Sm^{3+} ions. Specifically, energy was transferred from the excited states of Dy^{3+} to Sm^{3+}, enhancing the overall emission spectrum and enabling the production of warm-white light.

C. Chen et al. investigated the development of a specific type of glass-ceramic material for white light-emitting diode technology [12]. The study focused on borosilicate glass-ceramics co-doped with dysprosium (Dy^{3+}) and samarium (Sm^{3+}), which were enhanced by the incorporation of $Na_5Y_9F_{32}$ nanocrystals. It was found that the emission color could be tuned from yellow to white by applying the excitation at different wavelengths. With an increase in the doping concentration of Sm^{3+} and a reduction in Dy^{3+}, the emission of Sm^{3+} was enhanced, resulting in the production of white light. The emission spectrum of the Sm^{3+}-doped samples, excited at a wavelength of 401 nm, showed several emission bands at 563, 600, 647, and 707 nm, corresponding to the $^4G_{5/2} \rightarrow {}^6H_{J/2}$ (J = 5, 7, 9, 11) transitions, respectively. The emission spectra of the co-doped glass-ceramic, when excited at 350 nm, exhibited three emission bands at 484, 575, and 665 nm, corresponding to the $^4F_{9/2} \rightarrow {}^6H_{J/2}$ (J = 15, 13, 11) transitions of Dy^{3+}, respectively. The energy transfer between Dy^{3+} and Sm^{3+} ions revealed in this study was a crucial process for producing white light in borosilicate glass.

Sintering is a process that can be used to compact or fuse glass particles by heat to form a solid mass [2]. This process is often carried out in a conventional furnace. Microwave heating is a densification sintering method that has gained a lot of interest. It is a novel method that employs microwave radiation to heat and sinter materials, predominantly metal powders and ceramics. This method differs significantly from conventional sintering processes, which depend on external heat sources. In microwave sintering, the materials absorb microwave radiation, generating heat internally rather than relying on surface heating from an external source. This results in more uniform heating throughout the material, which may enhance the properties of the final product. In addition, it also has short processing times and high energy efficiency, making it a potential method for glass manufacturing.

K. Ashis et al. investigated the application of microwave radiation for the synthesis of iron-doped alumino-phosphate glass [13]. The study showed that the microwave method reduced the melting time to less than 2 h, compared to the 6–7 h required by conventional methods. Moreover, the glass produced using microwave radiation exhibited comparable structural and optical properties to that produced by conventional heating methods, confirming the effectiveness of microwave processing. Although the microwave-assisted synthesis or the sintering of materials is faster and energy-efficient, not all materials can effectively interact with microwave radiation. Silicate glasses are typically transparent to microwaves and cannot be directly heated by them at low temperatures. At high temperatures, they may absorb microwave radiation due to structural relaxation, resulting in further heating [14]. Therefore, the microwave heating of glass frequently requires a

microwave susceptor, such as silicon carbide (SiC), to initiate the heating process until the glass can absorb microwaves independently.

This research, therefore, focuses on tuning the emission color of borosilicate waste glasses by varying the doping ratios of Dy_2O_3 and Sm_2O_3 as well as the excitation wavelength. The study also addresses the use of microwave heating as an effective, rapid, and energy-efficient method for sintering glass samples, offering an alternative to conventional sintering method.

2. Materials and Methods

The glass waste was collected from broken laboratory glassware inside the department at Silpakorn University. Table 1 presents the chemical composition of the glass waste, confirming that it is borosilicate glass. After the collection of glass waste, the glass was carefully cleaned and allowed to dry in air. It was then crushed into small fragments and ground in a ball mill using alumina balls, occupying about three to four portions of the mill jar. The rotation velocity was set at 700 revolutions per minute for a duration of 4 h. Subsequent to milling, the resultant glass powder was sieved through a 325-mesh sieve (particle size of 44 μm).

Table 1. Chemical composition of the glass waste.

Component	Weight%	Component	Weight%
B_2O_3	14.83	K_2O	0.44
Na_2O	3.74	CaO	0.03
Al_2O_3	2.53	TiO_2	0.03
SiO_2	78.20	Fe_2O_3	0.04
P_2O_5	0.01	PbO	0.06
MgO	0.01	Total	99.92

Borosilicate glass powder and rare earth compounds, Dy_2O_3 (Sigma Aldrich, St. Louis, MO, USA, 99.9%) and Sm_2O_3 (Sigma Aldrich, 99.9%), were dried in an oven at 80 °C and then weighed as detailed in Table 2. They were then wet-mixed together in an ethanol medium using a mortar and pestle. The mixed powder was compacted into pellets using a hydraulic press at a pressure of 1.5 tons for 90 s. The obtained pellets were about 1.5 cm in diameter. The specimens, designated MD1–MD5, were then placed in a microwave kiln (inner dimension: Ø8 × 4.5 cm) and subjected to sintering in a household microwave oven at 800 W for 15 min. The microwave kiln is internally coated with silicon carbide, allowing it to absorb microwaves and produce heat. After sintering, all samples were characterized to determine their properties. The undoped glass (MD0) was also prepared by both conventional and microwave sintering processes for comparative analysis.

Table 2. Composition of the glass samples.

Sample	Composition		
	Borosilicate Powder (g)	Dy_2O_3 (g)	Sm_2O_3 (g)
MD0	3.00	0	0
MD1	2.94	0.06	0
MD2	2.94	0.04	0.02
MD3	2.94	0.03	0.03
MD4	2.94	0.0.2	0.04
MD5	2.94	0	0.06

The apparent and bulk densities were determined using the Archimedes principle. The following equations are used in the calculations:

$$\text{Apparent density} = W_D/(W_D - W_I) \quad (1)$$

$$\text{Bulk density} = W_D/(W_S - W_I) \quad (2)$$

where W_D is the dry weight of the glass sample, W_I is the weight of the glass sample when immersed in water, and W_S is the saturated weight after submerging in water. A Shimadzu XRD-6100 X-ray diffractometer (Kyoto, Japan) was used to analyze the crystallinity of the glass samples. The data were gathered in the 2-theta range of 10–60° with a voltage of 30 kV and a current of 20 mA at room temperature. The FTIR spectra were recorded in the range of 400–2200 cm^{-1}, using a Vertex 70v FT-IR spectrometer (Bruker, Leipzig, Germany). The surface morphology was observed with a scanning electron microscope (Tescan Mira3 FEG-SEM, Brno–Kohoutovice, Czech Republic). UV–Vis–NIR absorption spectra were measured in the wavelength range of 200–1800 nm using a UV–Vis–NIR spectrophotometer (Shimadzu UV-3600 Plus, Kyoto, Japan). Excitation and emission spectra were obtained using a Horiba Scientific FluoroMax+ spectrofluorometer (Kyoto, Japan).

3. Results and Discussion

Figure 1 illustrates the physical and structural properties of undoped glasses sintered with conventional heating at different temperatures for one hour and microwave heating at 800 W for varying durations. The results indicate that the properties of microwave- and conventionally sintered glass samples are comparable, suggesting that microwave heating can effectively be utilized for glass sintering. Based on XRD analysis, sintering via the conventional method, however, is likely to promote the crystallization of the cristobalite phase, which may affect both the mechanical and optical properties of the glasses. The SEM images also show that the samples prepared by the microwave sintering technique exhibit better quality compared to those subjected to conventional sintering [15]. The conventional heating method requires a temperature as high as 1100 °C to obtain smooth and homogeneous glass samples. Microwave heating is, therefore, a potential technique with uniform heating and low energy consumption for the sintering process. For the microwave sintering of doped glasses, a 15-min sintering time has been used.

Figure 2 compares the physical characteristics of glass samples doped with different concentrations of Dy^{3+} and Sm^{3+} and sintered in a microwave oven for 15 min under both daylight and UV irradiation. The uniformity and smooth, rounded surface of the borosilicate glass samples indicate that glass melting initiates during the sintering period. The smooth surface of the glass samples is attributed to uniform heating facilitated by microwave sintering. When examined in the dark under UV light, the samples exhibit visible luminescence with the emission color varying according to the concentrations of Dy^{3+} and Sm^{3+}.

The density of the doped glasses was measured using the Archimedes method. This is an important fundamental property that can be used to determine the structure of glasses and the quantity of porosities. The apparent and bulk densities of the doped glass samples prepared in a microwave oven are shown in Figure 3. The densities vary from 1.59 to 1.92 g/cm^3 and 1.58 to 1.91 g/cm^3, respectively, depending on the $Dy^{3+}-Sm^{3+}$ concentrations. Although the density of glass samples increases with higher Dy^{3+} content, it is still much lower than that of undoped glass. This could be because the incorporation of Dy^{3+} and Sm^{3+} into the borosilicate glass matrix might induce the porosities and the formation of non-bridging oxygen (NBO). The high density of the glass matrix in Dy^{3+}-doped glass relative to Sm^{3+}-doped glass can be ascribed to the greater molecular weight

of Dy_2O_3 in comparison to Sm_2O_3. Additionally, Dy^{3+} ions may be substituted inside the glass network. According to earlier studies, Dy^{3+} can replace borate ions, resulting in an increase in the density of the glass [16].

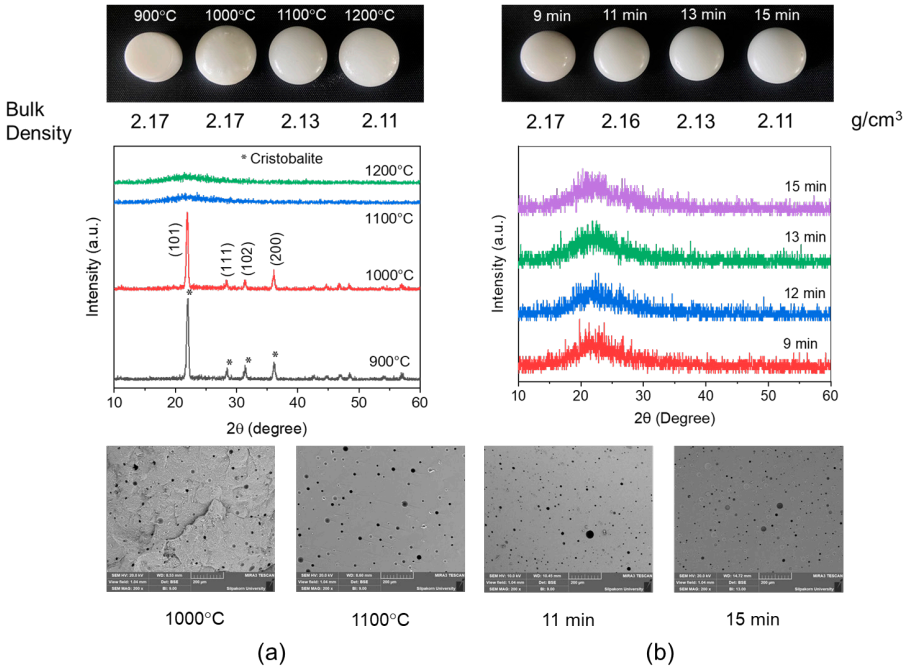

Figure 1. The physical and structural properties of undoped glasses sintered by (**a**) the conventional sintering method at different temperatures for 1 h and (**b**) the microwave sintering method at 800 W for different durations.

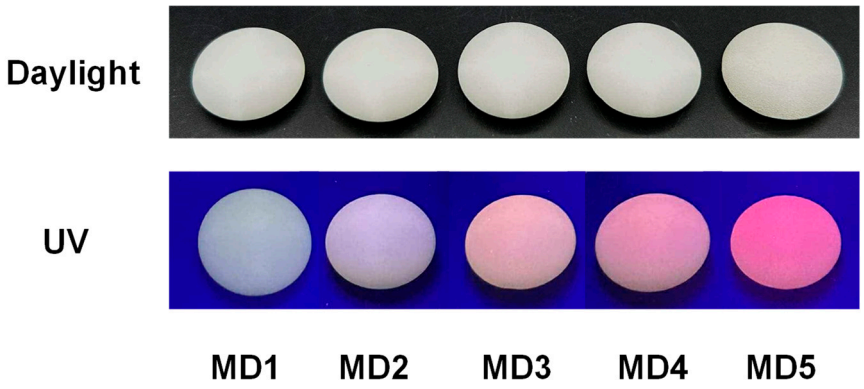

Figure 2. Digital images of glass samples under daylight and UV irradiation.

Figure 4 shows the XRD patterns of the glass samples. The powdered samples were prepared for XRD analysis by hammer crushing and grinding with a mortar and pestle. All samples exhibit a broad hump centered at about 22.5°, indicating that the glass is amorphous and lacks the long-range order. This indicates that the crystallization is not induced by the addition of doping oxides. The formation of a crystalline cristobalite phase is often observed in the current glass system prepared by the conventional sintering method, as shown in Figure 1. The results are consistent with previous studies on the microwave sintering of red-emitting glasses [2].

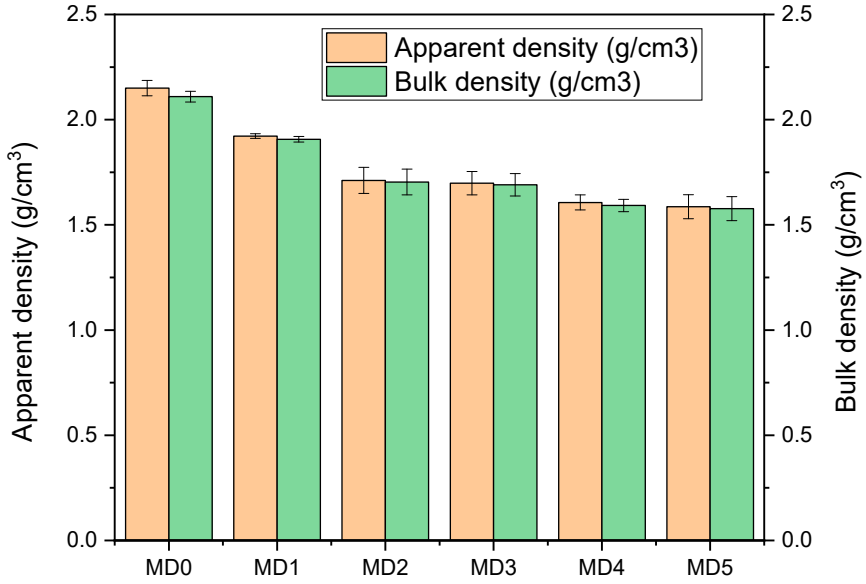

Figure 3. Apparent density of Dy^{3+}- and Sm^{3+}-doped glass samples.

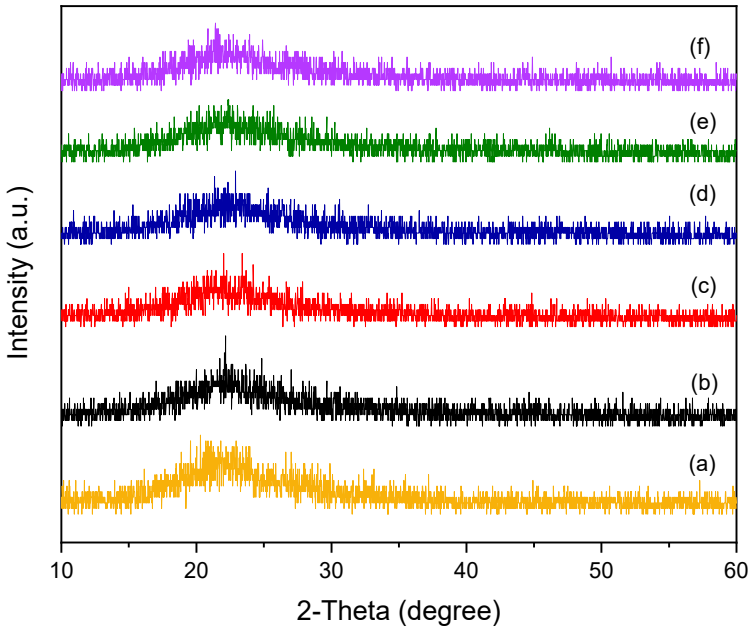

Figure 4. XRD patterns of (**a**) MD0, (**b**) MD1, (**c**) MD2, (**d**) MD3, (**e**) MD4, and (**f**) MD5.

The FTIR spectra of the glass samples are illustrated in Figure 5. The spectra reveal peaks at 465 cm^{-1}, 670 cm^{-1}, 793 cm^{-1}, 905 cm^{-1}, 1089 cm^{-1}, and 1414 cm^{-1}, corresponding to various vibrational modes: the bending vibration of Si-O-Si, the bending vibration of bridging oxygen [BO_3], the symmetric stretching of O-Si-O, the vibration of Si-B-O bonds in [BO_4], the symmetric stretching of [BO_3] and [BO_4] groups overlapped with the symmetric stretching of Si-O-Si, and the symmetric stretching vibration of B-O bonds in [BO_3] groups, respectively [17,18]. It can be clearly seen that the spectra of the doped glasses and the undoped glasses are very similar. This suggests that the incorporation of Dy^{3+} and Sm^{3+} into the borosilicate glass matrix does not alter the glass network. The band appearing at 1089 cm^{-1} of the undoped glasses, however, appears to be more intense, indicating a larger BO_3 content. In other words, the doping could potentially lead to the formation of non-bridging oxygens (NBOs) [19]. The appearance of NBOs in borosilicate glasses could be related to either Si and B units.

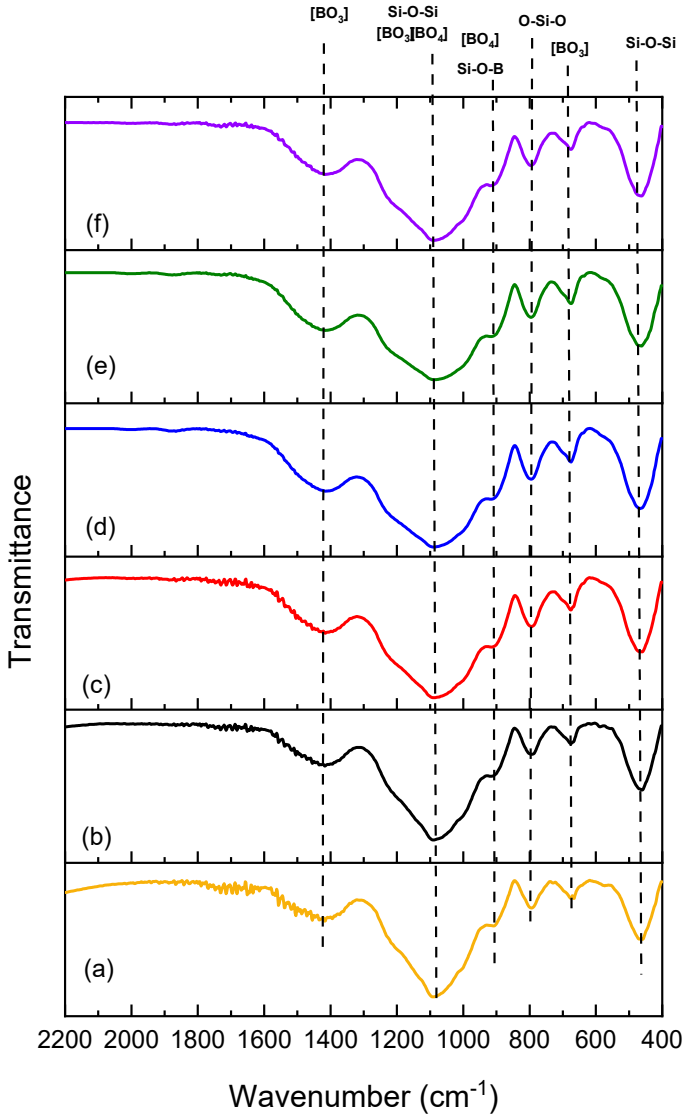

Figure 5. FTIR spectra of (**a**) MD0, (**b**) MD1, (**c**) MD2, (**d**) MD3, (**e**) MD4, and (**f**) MD5.

Figure 6 illustrates the absorption spectra of borosilicate glass doped with Dy^{3+} and Sm^{3+}. The Dy^{3+}-doped glass sample (MD1) (Figure 6a) exhibits four characteristic peaks at 894, 1081, 1256, and 1668 nm, corresponding to energy transitions from the ground state $^6H_{15/2}$ to states $^6F_{7/2}$, $^6F_{9/2}$, $^6F_{11/2}$ + $^6H_{9/2}$, and $^6H_{11/2}$ of Dy^{3+}, respectively. The most prominent transition occurs at 1256 nm due to the $^6H_{15/2}$-$6F_{11/2}$ + $^6H_{9/2}$ transition. On the other hand, the light absorption spectrum of the glass sample doped with Sm^{3+} (MD5) shows seven characteristic peaks at 402, 1074, 1223, 1367, 1470, 1524, and 1597 nm. The observed peaks are ascribed to energy transitions from the ground state $^6H_{5/2}$ to the excited states $^6P_{3/2}$, $^6F_{9/2}$, $^6F_{7/2}$, $^6F_{5/2}$, $^6F_{3/2}$, $^6H_{15/2}$, and $^6F_{1/2}$ of Sm^{3+}, respectively [11,12,20]. The absorption peaks at high energy (less than 400 nm) for both Dy^{3+} and Sm^{3+} are overlapped with the absorption band of glass.

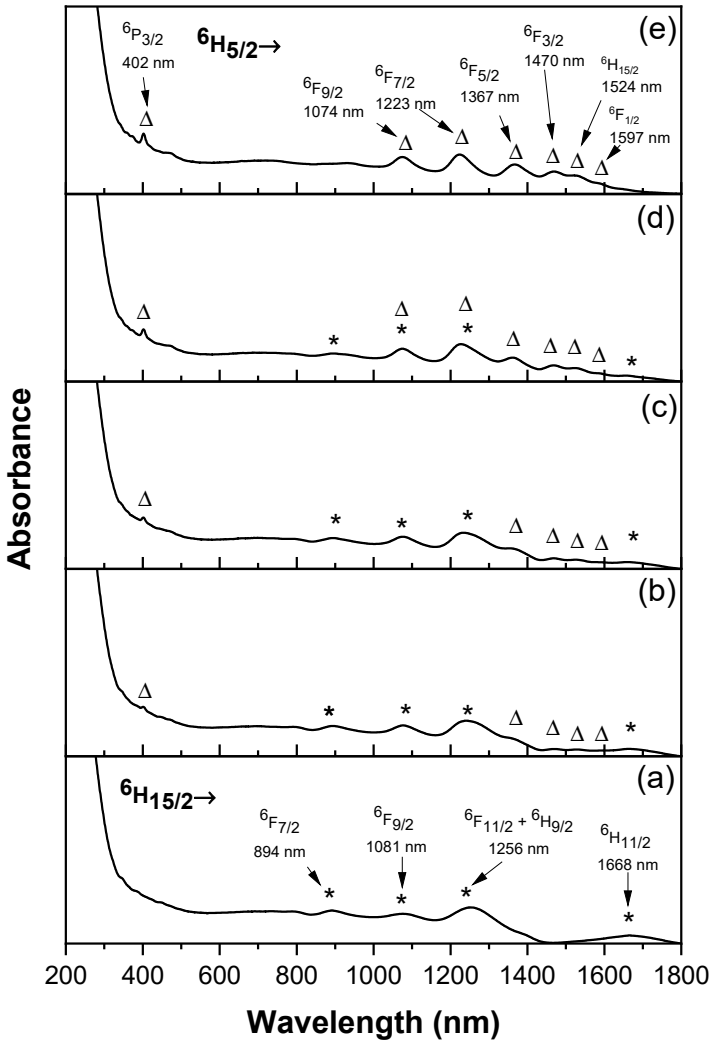

Figure 6. Absorption spectra of (**a**) MD1, (**b**) MD2, (**c**) MD3, (**d**) MD4, and (**e**) MD5. (*—Dy^{3+}, Δ—Sm^{3+}).

When a small quantity of Sm_2O_3 is added to Dy^{3+}-doped glass, the absorption peaks corresponding to Sm^{3+} are not clearly evident, as shown in Figure 6b. With an increase in Sm_2O_3 concentration in the glass, the more intense absorption peaks of Sm^{3+} are observed and attributed to the transitions from the ground state $^6H_{5/2}$ to various excited states. These are similar to those seen in a single Sm^{3+}-doped glass samples, as depicted in Figure 6b–e.

Figure 7 presents the morphology of the fracture surfaces of the glass samples. None of the samples exhibit crystal-like structures in the glassy phase matrix. The surface is uniform and homogeneous. However, the porosity of the glass is observable at a magnification of 200X. The pores appear to expand and increase in size with the doping and the increased concentration of Sm^{3+}, leading to a reduction in density. The introduction of an appropriate concentration of co-doping ions (MD4), however, may lead to a decrease in pore size. The porosity and the pore size can significantly affect light scattering and the optical properties of phosphor in glasses. Previous studies have shown that small pores (less than 2 μm) and low porosity can contribute to high luminescent efficiency [21]. The pore size and porosity can be controlled by modifying the particle size of the glass powder and the concentration of rare-earth elements in the glass matrix [21]. In addition, the mechanical properties of glass samples generally decrease with increasing porosity. As a result, it is essential to conduct a proper sintering process to ensure the full densification.

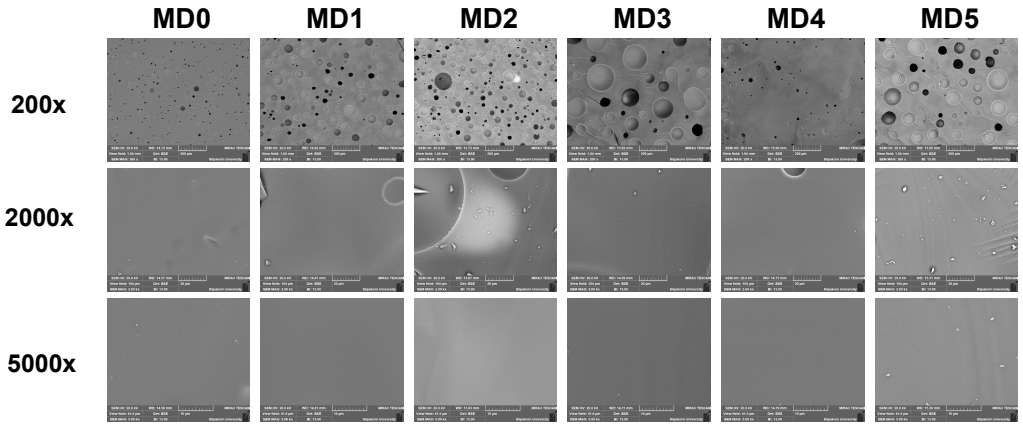

Figure 7. SEM images of glass samples' fractured surfaces.

The excitation and emission spectra of the doped glasses are displayed in Figures 8 and 9. In general, Dy^{3+}- and Sm^{3+}-doped glasses exhibit efficient excitation at wavelengths of 326–389 nm and 400–405 nm, respectively [21,22]. The excitation spectra of the MD1–MD5 samples at the emission wavelength of 601 nm, which is the optimal peak emission of Sm^{3+}, are shown in Figure 8a. It is found that the excitation spectrum of the Dy^{3+}-doped sample (MD1) contains a broad and weak band ranging from 300–475 nm, which corresponds to the characteristic f-f transition of Dy^{3+}. The maximum intensity in the excitation spectrum appears at 347 nm for the $^6H_{5/2}$-to-$^6P_{7/2}$ transition. The excitation spectra of the Sm^{3+}-doped samples (MD5) shows several characteristic transitions: $^6H_{5/2}$ to $^4H_{9/2}$ + $^4D_{7/2}$ (344 nm), $^6P_{5/2}$ + $^4D_{3/2}$ (362 nm), $^6P_{7/2}$ (375 nm), $^4F_{7/2}$ + $^6P_{3/2}$ (401 nm), and $^4I_{13/2}$ + $^4I_{11/2}$ + $^4I_{9/2}$ (450–490 nm) [23–25]. The most intense excitation peak is observed at 401 nm, which is, therefore, selected as the excitation wavelength for emission spectra. The MD2–MD4 samples co-doped with Dy^{3+} and Sm^{3+} exhibit excitation peaks similar to those of Sm^{3+}. This indicates that the excited states of Dy^{3+} do not significantly result in emission at 601 nm.

Under the 401 nm excitation (Figure 8b), the emission spectrum of MD5 exhibits three prominent emission peaks located at approximately 562, 601, 647, and 711 nm due to the transition from $^4G_{5/2}$ to $^6H_{5/2}$, $^6H_{7/2}$, $^6H_{9/2}$, and $^6H_{11/2}$ of Sm^{3+}, respectively. The highest emission occurs at 601 nm, which is the characteristic and the most intense emission peak of Sm^{3+} [26]. The doublet peaks associated with each characteristic emission arises from variations in the samarium sites or different crystal fields [27]. For the co-doped glass samples, the emission spectra are similar to that of the MD5 sample. The intensity of the emission peaks increases with the increasing amount of Sm^{3+}. A Dy^{3+} emission peak (575 nm) is also observed at low intensity and superimposed on the bands of the Sm^{3+} emission. For the MD1 sample, the emission spectrum in the wavelength range of 500–750 nm shows a board emission peak centered at 575 nm (yellow region) due to the $^4F_{9/2}$-$^6H_{13/2}$ transition. In general, Dy^{3+} ions exhibit emission bands at 480 nm (blue) and 580 nm (yellow).

To further understand the energy transfer mechanism between Dy^{3+} and Sm^{3+}, the excitation and emission spectra are investigated under the 574 nm emission and the 388 nm excitation wavelengths, respectively. Figure 9a shows the excitation spectra at an emission wavelength of 574 nm, which is the peak emission of Dy^{3+}. In the MD5 sample, excitation peaks are observed at wavelengths of 344, 363, 375, 404, and 400–490 nm due to energy level transitions from $^6H_{5/2}$ to $^4H_{9/2}$ + $^4D_{7/2}$, $^6P_{7/2}$ + $^4D_{3/2}$, $^6P_{7/2}$, $^4F_{7/2}$ + $^6P_{3/2}$, and $^4I_{13/2}$ + $^4I_{11/2}$ + $^4I_{9/2}$ of Sm^{3+}, respectively. In the MD1 sample, excitation peaks occur at wavelengths of 328, 346, 369, 388, 427, and 443 nm. These are due to energy level transitions from $^6H_{15/2}$ to $^4M_{17/2}$, $^6P_{7/2}$, $^6P_{5/2}$, $^4I_{13/2}$, $^4G_{11/2}$, and $^4I_{15/2}$ of Dy^{3+}, respectively [23–25].

The most intense excitation peak at a wavelength of 388 nm was then chosen to stimulate light emission for the analysis of co-doped samples.

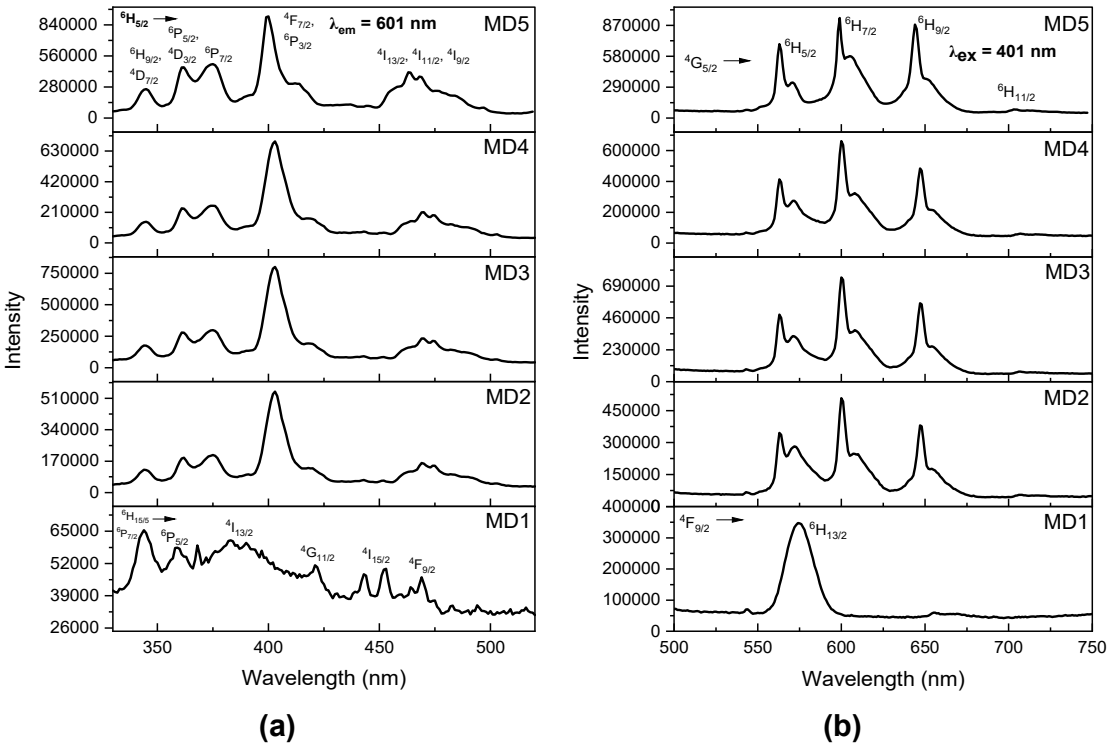

Figure 8. (**a**) Excitation spectra monitoring at 601 nm emission wavelength and (**b**) emission spectra monitoring at 401 nm excitation wavelength of Dy^{3+}- and Sm^{3+}-doped glass samples.

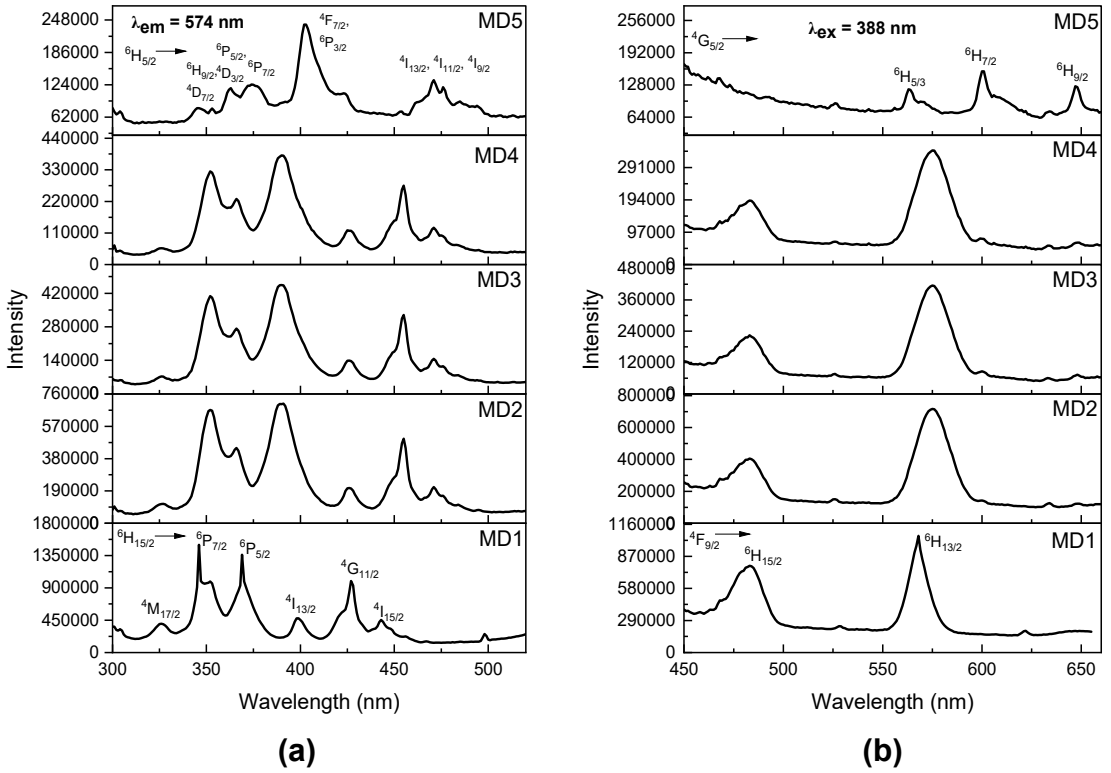

Figure 9. (**a**) Excitation spectra monitoring at 574 nm emission wavelength and (**b**) emission spectra monitoring at 388 nm excitation wavelength of Dy^{3+}- and Sm^{3+}-doped glass samples.

The emission spectra of the single doped sample under ultraviolet light emission (388 nm) exhibits characteristic peaks of doping ions, as shown in Figure 9b. For Dy^{3+}, there are two emission peaks located at 483 nm (blue region) and 568 nm (yellow region), corresponding to the magnetic dipole $^4F_{9/2}$-$^6H_{15/2}$ transition and electronic dipole $^4F_{9/2}$-$^6H_{13/2}$ transition of Dy^{3+}, respectively [28–30]. The single Sm^{3+}-doped glass exhibits three characteristic red emission peaks at 564, 601, and 647 nm, which corresponds to the transition from $^4G_{5/2}$ to $^6H_{5/2}$, $^6H_{7/2}$, and $^6H_{9/2}$, respectively. These peaks, however, exhibit low intensity due to the unfavorable excitation at 388 nm for Sm^{3+} emission. In co-doped glasses, it is evident that the peak of Sm^{3+} emission is nearly absent. A very weak peak is observed at approximately 600 nm due to the $^4G_{5/2}$-$^6H_{7/2}$ transition of Sm^{3+}. The emission peak associated with the $^4F_{9/2}$-$^6H_{13/2}$ transition of Dy^{3+}, however, shifts to a longer wavelength (575 nm), and the emission intensity decreases with the addition of Sm^{3+}. When the electrons at the ground state $^6H_{15/2}$ of Dy^{3+} absorb energy at 388 nm, they are excited to a higher energy level. These unstable electrons subsequently drop to the lower energy state $^4F_{9/2}$ through a nonradiative transition process, followed by the radiative transitions to the states $^6H_{15/2}$ and $^6H_{13/2}$, resulting in yellow and blue emissions. Lower wavelength excitation light possesses higher energy, which more effectively stimulates Dy^{3+} emission. However, the emission intensity depends on the concentration of Dy^{3+}. The peak shift is likely attribute to an increase in non-bridging oxygens (NBOs) resulting from co-doping.

Based on the current findings, the excitation is most efficient when employing light of a particular wavelength. Excitation at a wavelength with high absorbance should produce multiple excited states, yielding strong fluorescence. The excitation spectra of the co-doped glass sample, however, may differ from those of single-doped glass samples. No evidence on the energy transfer from Dy^{3+} ions to Sm^{3+} ions is obtained in this study for the co-doping of Dy^{3+} and Sm^{3+}. Despite the overlap between the emission peak of Dy^{3+} and the excitation peak of Sm^{3+}, as shown in Figure 10, the energy transfers from Dy^{3+} to Sm^{3+} may be transferred back to the Dy^{3+}, thereby inhibiting emission in Sm^{3+} [31].

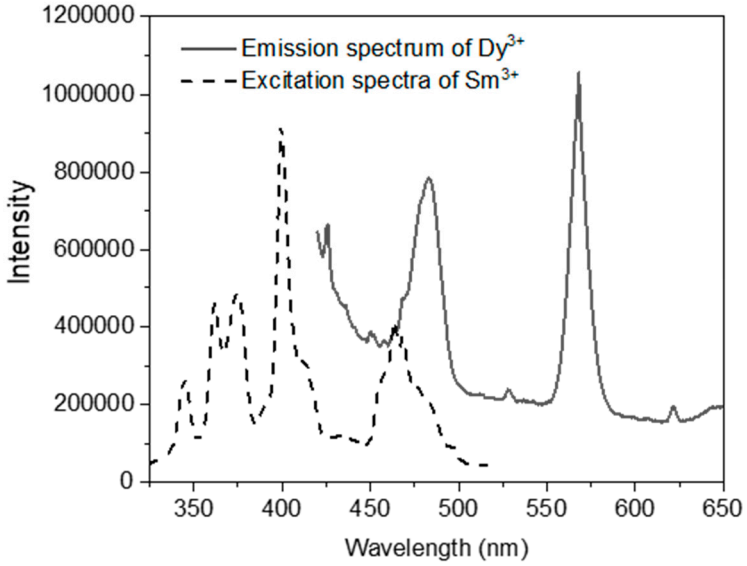

Figure 10. The overlap between the emission spectrum of MD1 (Dy^{3+}) and excitation spectra of MD5 (Sm^{3+}).

Nevertheless, it can be seen that the emission color can be tuned by employing different excitation wavelengths in the co-doped glasses [20]. Figure 11 shows the CIE 1931 chromaticity diagrams corresponding to different excitation wavelengths. It can be clearly seen that the variation in excitation wavelengths significantly affects the chromaticity

coordinate values. With the optimized excitation at 388 nm, the emitted light from the Dy^{3+}-doped glasses is observed in white region. The chromaticity coordinates of the Sm^{3+}-doped glasses, on the other hand, are located in the yellow light region of the CIE 1931 chromaticity diagram with the excitation at 401 nm. The co-doping enhances light emission predominantly in the white and yellowish-orange region for excitations at 388 nm and 401 nm, respectively. The adjustment of emitting color can be accomplished by modifying the excitation wavelength and the doping ratios.

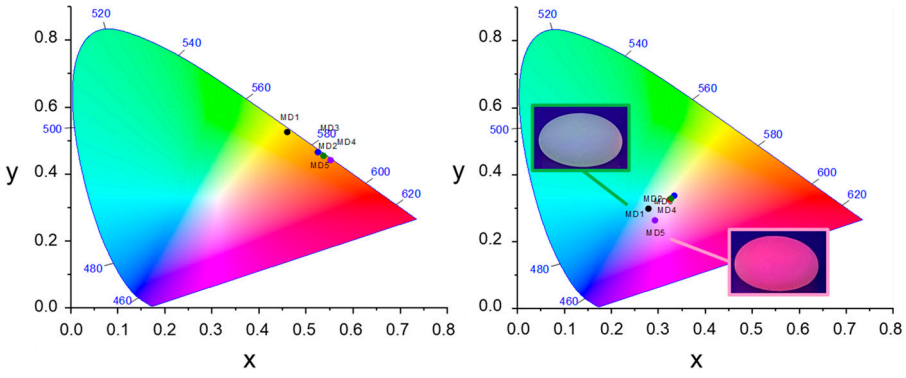

Samples	λ_{ex} = 401 nm		λ_{ex} = 388 nm	
	x	y	x	y
MD1	0.460	0.525	0.279	0.298
MD2	0.525	0.465	0.324	0.325
MD3	0.531	0.459	0.334	0.337
MD4	0.537	0.454	0.327	0.328
MD5	0.552	0.441	0.293	0.263

Figure 11. CIE 1931 Chromaticity diagram of Dy^{3+}- and Sm^{3+}-doped glass samples under excitation at (**a**) 401 nm and (**b**) 388 nm.

4. Conclusions

This study investigated the application of microwave sintering for the preparation of fluorescent glasses doped with Dy^{3+} and Sm^{3+} in varying proportions. The results indicate that the surface of the prepared glass appeared smooth without the formation of crystalline phases. The study on the effects of doping Dy^{3+} and Sm^{3+} ratios suggests that the introduction of these doping ions increases the porosity and the density of the glasses. Under 401 nm excitation, emission peaks of Sm^{3+} and co-doped glasses occur at 562, 601, 647, and 711 nm, corresponding to the transitions from $^4G_{5/2}$ to $^6H_{5/2}$, $^6H_{7/2}$, $^6H_{9/2}$, and $^6H_{11/2}$ of Sm^{3+}, respectively. However, under 388 nm excitation, no energy transfer from Dy^{3+} to Sm^{3+} is evident. The emission corresponds to the energy transitions ($^4F_{9/2}$-$^6H_{15/2}$, and $^4F_{9/2}$-$^6H_{13/2}$) of Dy^{3+}, and the intensity decreases with increasing Sm^{3+} concentrations.

Author Contributions: Conceptualization, A.B. (Achanai Buasri) and V.L.; methodology, A.B. (Achanai Buasri) and V.L.; software, V.L.; validation, A.B. (Achanai Buasri), A.B. (Apichaya Boonpanya), A.Y., T.K. and V.L.; formal analysis, A.B. (Achanai Buasri), A.B. (Apichaya Boonpanya), A.Y., T.K. and V.L.; investigation, A.B. (Apichaya Boonpanya), A.Y. and T.K.; resources, A.B. (Achanai Buasri) and V.L.; data curation, A.B. (Achanai Buasri) and V.L.; writing—original draft preparation, A.B. (Achanai Buasri) and V.L.; writing—review and editing, A.B. (Achanai Buasri) and V.L.; visualization, V.L.; supervision, V.L.; project administration, V.L.; funding acquisition, A.B. (Achanai Buasri) and V.L. All authors have read and agreed to the published version of the manuscript.

Funding: This research was financially supported by the Thailand Science Research and Innovation (TSRI): National Science, Research and Innovation Fund (NSRF) (Fundamental Fund: Fiscal Year 2024: Grant No. 196003).

Data Availability Statement: All the data are available from the corresponding author.

Acknowledgments: The authors also wish to thank the Department of Materials Science and Engineering, Faculty of Engineering and Industrial Technology, Silpakorn University for supporting and encouraging this investigation.

Conflicts of Interest: The authors declare no conflicts of interest.

References

1. Choi, S.H.; Bin Kwon, S.; Yoo, J.H.; Na, M.; Kim, B.Y.; Yoon, H.; Park, S.H.; Kinski, I.; Kang, B.K.; Yoon, D.H.; et al. Fabrication of phosphor in glass using waste glass for automotive lighting application. *Sci. Rep.* **2023**, *13*, 1–8. [CrossRef] [PubMed]
2. Buasri, A.; Keereekongsakol, W.; Phuttharaksa, U.; Loryuenyong, V. Microwave heating for the production of red-emitting sintered waste glass containing rare-earth ions. *Results Opt.* **2024**, *15*. [CrossRef]
3. Loryuenyong, V.; Buasri, A. Preparation of Luminescent Glass Aggregates from Soda-Lime Waste Glass. *Int. J. Photoenergy* **2021**, *2021*, 1–6. [CrossRef]
4. Lopez, R.; El-Fata, C. Environmental implications of using waste glass as aggregate in concrete. *J. Compos. Sci.* **2024**, *8*, 507. [CrossRef]
5. Loryuenyong, V.; Panyachai, T.; Kaewsimork, K.; Siritai, C. Effects of recycled glass substitution on the physical and mechanical properties of clay bricks. *Waste Manag.* **2009**, *29*, 2717–2721. [CrossRef] [PubMed]
6. Hasan, R.; Siddika, A.; Akanda, P.A.; Islam, R. Effects of waste glass addition on the physical and mechanical properties of brick. *Innov. Infrastruct. Solutions* **2020**, *6*, 1–13. [CrossRef]
7. Fanache, M.; Vasiliu, L.; Harja, M. Composite materials with glass fiber waste and blast furnace slag. *J. Compos. Sci.* **2024**, *8*, 256. [CrossRef]
8. Bharat, L.K.; Jeon, S.-K.; Krishna, K.G.; Yu, J.S. Rare-earth free self-luminescent $Ca_2KZn_2(VO_4)_3$ phosphors for intense white light-emitting diodes. *Sci. Rep.* **2017**, *7*, srep42348. [CrossRef] [PubMed]
9. Sarkar, S.; Dutta, S.; Azam, S.; Singha, D.K.; Mondal, S.K.; Mahata, P. Design and synthesis of a series of rare-earth coordination polymer-based phosphors: Exploration of the white light emission property. *ACS Appl. Opt. Mater.* **2024**. [CrossRef]
10. Pamuluri, H.; Rathaiah, M.; Linganna, K.; Lavin, V.; Venkatramu, V. Role of $Dy^{3+} \rightarrow Sm^{3+}$ energy transfer in the tuning of warm to cold white light emission in Dy^{3+}/Sm^{3+} co-doped $Lu_3Ga_5O_{12}$ nano-garnets. *New J. Chem.* **2018**, *42*, 1260–1270. [CrossRef]
11. Yan, W.; Li, J.; Zhang, W.; Gao, X.; Zhang, P. Warm-white luminescence of Dy^{3+} and Sm^{3+} co-doped $NaSrPO_4$ phosphors through energy transfer between rare earth ions. *J. Mater. Sci. Mater. Electron.* **2021**, *32*, 16648–16661. [CrossRef]
12. Chen, C.; Yu, C.; Xu, F.; Li, Q.; Zhang, Y. High energy transfer in Dy^{3+}/Sm^{3+} co-doped transparent borosilicate glass-ceramics containing novel $Na_5Y_9F_{32}$ nanocrystals for w-LEDs applications. *Ceram. Int.* **2020**, *47*, 1–9. [CrossRef]
13. Mandal, A.K.; Biswas, K.; Annapurna, K.; Guha, C.; Sen, R. Preparation of alumino-phosphate glass by microwave radiation. *J. Mater. Res.* **2013**, *28*, 1955–1961. [CrossRef]
14. Ghussn, L.; Martinelli, J.R. A novel method to produce niobium phosphate glasses by microwave heating. *J. Mater. Sci.* **2004**, *39*, 1371–1376. [CrossRef]
15. Nemala, S.S.; Ravulapalli, S.; Mallick, S.; Bhargava, P.; Bohm, S.; Bhushan, M.; Thakur, A.K.; Mohapatra, D. Conventional or microwave sintering: A comprehensive investigation to achieve efficient clean energy harvesting. *Energies* **2020**, *13*, 6208. [CrossRef]
16. Zaman, F.; Khan, I.; Khattak, S.; Kaewkhao, J.; Ataullah; Shoaib, M.; Shah, A.; Rooh, G. Investigation of luminescence and lasing properties of Dy^{3+}-doped-borate glasses for white light generation. *Solid State Sci.* **2019**, *90*, 68–75. [CrossRef]
17. Konon, M.; Polyakova, I.G.; Mazur, A.S.; Saratovskii, A.S.; Danilovich, D.P.; Alikin, M. Crystallization of cristobalite in sodium borosilicate glass in the presence of Cr_2O_3. *Materials* **2023**, *16*, 5016. [CrossRef]
18. Ling, Z.; Wang, A. Raman spectroscopic study of quartz in lunar soils from apollo 14 and 15 missions. In Proceedings of the 40th Annual Lunar and Planetary Science Conference, The Woodlands, TX, USA, 23–27 March 2009.
19. Zhang, Q.; Su, G. Preparation of amino functional polysiloxane–lanthanide (Dy^{3+} and Sm^{3+}) composites. *Polym. Polym. Compos.* **2019**, *27*, 279–286. [CrossRef]
20. Fernández-Rodríguez, L.; Balda, R.; Fernández, J.; Durán, A.; Pascual, M.J. Structure and luminescent properties of Sm/Dy-doped $Sr_2MgSi_2O_7$ glass–ceramics. *Int. J. Appl. Glas. Sci.* **2022**, *14*, 140–154. [CrossRef]
21. Sharma, S.; Brahme, N.; Bisen, D.P.; Dewangan, P. Cool white light emission from Dy^{3+} activated alkaline alumino silicate phosphors. *Opt. Express* **2018**, *26*, 29495–29508. [CrossRef] [PubMed]

22. Shih, H.-R.; Chang, Y.-S. Structure and photoluminescence properties of Sm^{3+} ion-doped $YInGe_2O_7$ phosphor. *Materials* **2017**, *10*, 779. [CrossRef] [PubMed]
23. Dixit, P.; Chauhan, V.; Rai, S.; Pandey, P.C. Realization of neutral white light emission in $CaMoO_4$:$4Dy^{3+}$ phosphor via Sm^{3+} co-doping. *J. Alloy. Compd.* **2022**, *897*. [CrossRef]
24. Li, P.; Zhang, X.; Zhang, J.; Qi, X.; Liu, X. Investigations of thermal stability and spectroscopic features of Sm^{3+} doped strontium aluminate glasses. *Coatings* **2021**, *12*, 3. [CrossRef]
25. Kumar, A.N.; Jnaneshwara, D.; Nagabhushana, H.; Pratapkumar, C.; Ravikumar, C.; Kumar, M.A.; Shekhar, T.S.; Prashantha, S. Photoluminescence, photocatalytic and electrochemical performance of $La_{10}Si_6O_{27}$:Sm^{3+} nanophosphor: It's applications in display, photocatalytic and electrochemical sensor. *Appl. Surf. Sci. Adv.* **2021**, *4*, 100070. [CrossRef]
26. Khan, I.; Shoaib, M.; Alsaiari, N.S.; Wabaidur, S.; Rooh, G.; Srisittipokakun, N.; Ullah, I.; Kaewkhao, J. Spectroscopic investigation of alkaline-earth borosilicate glasses doped with Sm_2O_3 for display devices application. *Optik* **2022**, *269*. [CrossRef]
27. Ryba-Romanowski, W.; Strzęp, A.; Lisiecki, R.; Berkowski, M.; Rodriguez-Rodriguez, H.; Martin, I.R. Effect of substitution of lutetium by gadolinium on emission characteristics of $(Lu_xGd_{1-x})_2SiO_5$: Sm^{3+} single crystals. *Opt. Mater. Express* **2014**, *4*, 739–752. [CrossRef]
28. Wu, H.; Sun, Z.; Gan, S.; Li, L. Luminescence properties of Dy^{3+} or/and Sm^{3+} doped $LiLa(WO_4)_2$ phosphors and energy transfer from Dy^{3+} to Sm^{3+}. *Solid State Sci.* **2018**, *85*, 48–53. [CrossRef]
29. Yang, Z.; Sun, Y.; Xu, Q.; Sun, J. Preparation and photoluminescence properties of Dy^{3+}-doped $Ba_3Lu(PO_4)_3$ phosphors. *J. Rare Earths* **2015**, *33*, 1251–1255. [CrossRef]
30. Henaish, A.M.; Hemeda, O.M.; Arrasheed, E.A.; Shalaby, R.M.; Ghazy, A.R.; Weinstein, I.A.; Darwish, M.A.; Trukhanova, E.L.; Trukhanov, A.V.; Trukhanov, S.V.; et al. Tailoring variations in the microstructures, linear/nonlinear optical, and mechanical properties of dysprosium-oxide-reinforced borate glasses. *J. Compos. Sci.* **2023**, *7*, 61. [CrossRef]
31. Holloway, W.W.; Kestigian, M. Energy Transfer between the Sm^{3+}, Eu^{3+}, Tb^{3+}, and Dy^{3+} Ions in Sodium Rare-Earth Tungstates. *J. Opt. Soc. Am.* **1966**, *56*, 1171–1174. [CrossRef]